TU Delft

Delft University of Technology

Optical and structural characterization of Tm_2O_3, TmN, and TmO_xN_y thin films grown by direct-current reactive magnetron sputtering

Meeuwissen, Axel; Bosco, Giacomo B.F.; van der Kolk, Erik

DOI
10.1016/j.tsf.2020.138450

Publication date
2021

Document Version
Final published version

Published in
Thin Solid Films

Citation (APA)
Meeuwissen, A., Bosco, G. B. F., & van der Kolk, E. (2021). Optical and structural characterization of Tm_2O_3, TmN, and TmO_xN_y thin films grown by direct-current reactive magnetron sputtering. *Thin Solid Films*, *717*, Article 138450. https://doi.org/10.1016/j.tsf.2020.138450

Important note
To cite this publication, please use the final published version (if applicable).
Please check the document version above.

Copyright
Other than for strictly personal use, it is not permitted to download, forward or distribute the text or part of it, without the consent of the author(s) and/or copyright holder(s), unless the work is under an open content license such as Creative Commons.

Takedown policy
Please contact us and provide details if you believe this document breaches copyrights.
We will remove access to the work immediately and investigate your claim.

This work is downloaded from Delft University of Technology.
For technical reasons the number of authors shown on this cover page is limited to a maximum of 10.

Thin Solid Films 717 (2021) 138450

Contents lists available at ScienceDirect

Thin Solid Films

journal homepage: www.elsevier.com/locate/tsf

Optical and structural characterization of Tm_2O_3, TmN, and TmO_xN_y thin films grown by direct-current reactive magnetron sputtering

Axel Meeuwissen, Giacomo B.F. Bosco *, Erik van der Kolk

Luminescence Materials Research group, Department of Radiation Science and Technology, Faculty of Applied Sciences, Delft University of Technology, Mekelweg 15, 2629 JB Delft, The Netherlands

ARTICLE INFO

Keywords:
Reactive magnetron direct-current sputtering
Thulium sesquioxide
Thulium mononitride
Thulium oxynitrides

ABSTRACT

This paper reports the fabrication and characterization of several thulium oxide and nitride thin films grown by reactive magnetron direct-current sputtering. Hysteresis curves of the Tm emission spectra of the sputtering plasma versus the flow of N_2 or O_2 around the Tm-metal target were monitored. Emission spectra of atomic transition lines in the region between 370 and 420 nm were identified to be of neutral thulium. The plasma emission was compared to the hysteresis curves generated by monitoring the sputter rate and target voltage. The nitride films' composition and optical properties were determined by X-Ray Diffraction, and optical transmission spectroscopy. The composition of the oxide films was determined by energy dispersive X-ray spectroscopy. The films are initially amorphous but crystallize after thermal treatment at 800°C. The optical bandgap values obtained using the Tauc method are consistent with what has been previously reported for both Tm_2O_3 and TmN prepared by other methods.

1. Introduction

Thulium sesquioxides (Tm_2O_3) have received some attention in recent years. Possible applications include Tm_2O_3 metal-oxide-semiconductor capacitors [1] and biosensors [2]. Moreover, research also has been dedicated to investigating their potential as a high-k dielectric material [1,3]. Several techniques have already been applied to produce it from, for example, atomic layer deposition [4,5], electron beam evaporation, or molecular beam epitaxy [3]. However, there is little data on optical properties of Tm_2O_3 thin films grown by magnetron sputtering.

Rare Earth mononitrides have potential in spintronics [6] due to the inherent strong magnetic properties of the elements from the rare earth family. While rare earth mononitrides have been reported for over 5 decades [7,8], only a few compounds have been reported by routes involving high vacuum growth techniques - particularly by employing epitaxial [9–11] growth, pulsed laser deposition [12], or direct current (DC) magnetron sputtering [6]. Despite being a very common technique for thin film growth, sputtering grown thulium nitride (TmN) thin films remained not yet demonstrated [13] nor its properties have been directly explored.

Although Tm oxides, nitrides and the sub-oxide(nitride) variants are interesting from an application point of view, the controlled reactive sputtering is complicated by a hysteresis behaviour of the Tm metal sputter target. During sputtering with reactive gases, Tm compound formation occurs at the surface of the sputtering target. In this so-called target poisoning regime, the target sputter rate is usually significantly lower than in the metallic regime [14,15].

Very often, the target condition depends on the operation history, so hysteresis effects between process parameters like plasma optical emission intensity, the target voltage, the sputter erosion rate and controllable sputter parameters such as the flow of reactive gases appear. The characterization of the hysteresis behaviour can be used as a tool in the controlled preparation of films with the correct stoichiometry or with sub-stoichiometric character. Currently, there is no available experimental information on the target poisoning behaviour of the Tm metal target in reactive DC sputtering. In this work, we show that the relationship between the reactive gas flow rate and the atomic Tm emission from the plasma is complex and nonlinear but is also capable of giving information on the metallic thulium target poisoning during sputtering.

In view of the limited available data this contribution offers synthesis and characterization data of Tm_2O_3, TmN, and TmO_xN_y thin films grown by DC magnetron sputtering. A description of the deposition system

* Corresponding author.
E-mail address: G.BizinotoFerreiraBosco@tudelft.nl (G.B.F. Bosco).

https://doi.org/10.1016/j.tsf.2020.138450
Received 5 May 2020; Received in revised form 2 November 2020; Accepted 19 November 2020
Available online 26 November 2020
0040-6090/© 2020 The Authors. Published by Elsevier B.V. This is an open access article under the CC BY license (http://creativecommons.org/licenses/by/4.0/).

used, and on the used characterization methods, are described in the experimental methods section. The characterization tools employed were X-ray diffraction (XRD), scanning electron microscopy (SEM), energy dispersive x-ray spectroscopy (EDS), optical transmission, and plasma emission spectroscopy. In the results and discussion section there is a description on the film properties depending on the deposition conditions. The properties were compared to the state of target poisoning by nitrogen or oxygen.

2. Experimental Details

A series of TmO_xN_y thin films were deposited on square 25.4 × 25.4 mm^2 UV grade quartz substrates at room temperature within an AJA ATC Orion 5 magnetron sputtering system with a base pressure of 2.0 × 10^{-7} Pa. Prior to the deposition, each substrate was cleaned by rinsing three times with DI water and ethanol. The deposition was carried out with 5.08 cm diameter Tm metal (99.99 %, Demaco) targets which were reactively co-sputtered with DC powers between 20 and 40 W for 9 or 12 h. The process total gas flow was kept fixed at 32 sccm. Multiple combinations of 6N purity Ar, 5N purity O_2 and 5N purity N_2 gas flows were chosen. Table 1 shows the specific parameters used for each film deposition. The working pressure was 0.4 Pa and the samples were not actively heated. To obtain homogeneous films, the substrate was continuously rotated at 60 rpm.

During deposition, the emission spectrum of the plasma was measured every three seconds and averaged five times with an Ocean Optics USB4000 spectrometer from an optical window located at the bottom of the sputter chamber, collecting light with a bare fibre. Thulium lines in these spectra were identified using NIST Atomic Spectra Database Lines [16]. This data can provide qualitative intensities for Thulium atomic spectral lines on Tm, Tm^+, and Tm^{2+}. Figure 1 shows one typical spectrum. The observed lines are dominated by neutral Thulium atomic transitions with a much smaller contribution from Tm^+, and Tm^{2+} transitions.

In order to choose the appropriate parameters of film deposition, hysteresis curves were generated. The O_2 or N_2 gas flow was systematically varied in steps of 0.2 sccm in one-minute intervals between each step, to produce a hysteresis curve displaying neutral Tm atomic emission line intensity versus gas flow.

Lines intensities were calculated by integrated emission spectra between 370 and 420 nm. The target voltage readings and deposition rate (monitored by a MCM-160 quartz crystal micro balance sensor) were stored in intervals of 2 *s*.

A JEOL IT-100 operated at 7 keV was used for SEM/EDS analysis. The energy of the electron beam was chosen to prevent beam penetration and subsequent characteristic X-ray emission from the quartz substrate (the thicknesses of the films, over 350 nm for the oxides, are beyond the x-ray penetration depth, at oxygen K-α energy, of about 20 nm [17]). Quantitative elemental analysis without a conductive coating was achieved by employing the device in low vacuum mode (35 Pa). Elemental compositions were quantified at 1000 × magnification. XRD measurements were performed using a PANalytical X'pert Pro MPD diffractometer in Bragg-Brentano geometry with a Cu Kα anode (λ = 0.1540598 nm) operating at 45 kV and 40 mA. A regular θ-2θ scan was performed with the film embedded in a sample spinner to reduce the effects of preferred orientation in the crystalline structure for TmO#1,

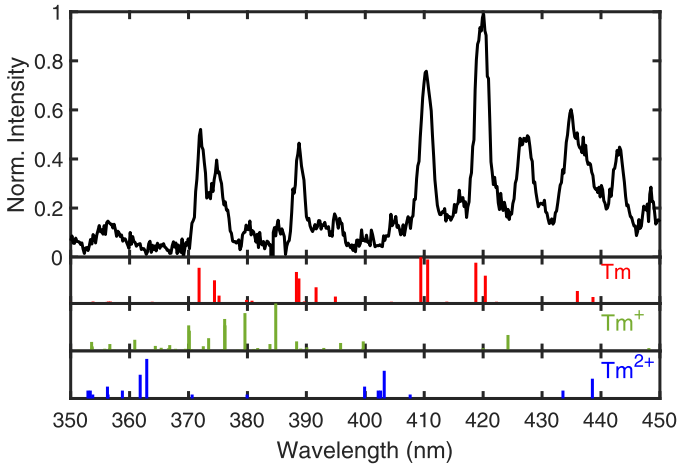

Figure 1. The upper graph shows the normalized plasma emission spectrum during deposition of sample TmO#2. It used 1.8 sccm of O_2 gas flow. Below, reference values for the atomic spectral lines corresponding to neutral Tm (red), Tm^+ (green), and Tm^{2+} (blue) [12]. Full description on deposition parameters are summarized at table 1.

TmON#1, and TmON#2. Due to the oxidizing nature, this setup could not be used for samples TmON#3 and TmN#1. Instead, the spinner was replaced by a custom made vacuum sealed sample holder with Kapton foil to prevent exposure to air.

The transmission was measured by placing the samples between a collimated (2.7 mm diameter) xenon light source and the entrance port of a 5.08 cm diameter integrating sphere (IS200-4, Thorlabs), with an Ocean Optics QEPro spectrometer (200 μm slit width) connected to the off-axis detector port. Transmission spectra were recorded with an integration time of 1s and averaged 10 times. Dark spectra were recorded by blocking the entrance of the integrating sphere with highly absorbing and reflecting Al tape. Lamp spectra were recorded by directly exposing the integrating sphere to the collimated light. The transmission spectra were corrected using these two reference measurements, measured with identical settings. See [18] for more details on the used transmission setup.

Films TmO#1, TmO#2, and TmON#2 showed little absorbance of visible light. For complete characterization of these thin films, transmission measurements in the vacuum ultraviolet region were performed. These samples were illuminated with a Deuterium lamp (ARC DS100) and the transmitted spectrum was detected using a vacuum monochromator (ARC VM504) with 0.15 mm slit width and a VUV-sensitive EMI 9426B photomultiplier tube.

A characteristic spectrum obtained with such a method in the visible region is shown graphically in figure 2. This spectrum was fitted using OPTIFIT [19]. It uses a combination of the Swanepoel method [20], the Sellmeier dispersion relation [21] and a review by Poelman and Smet [22] to determine thickness and refractive index - the substrate refractive index at 585 nm was fixed to the known 1.45 value of UV grade quartz [23]. The Tauc method was applied to characterize the films' optical bandgaps (E_{Tauc}).

Before XRD measurements, the films were annealed so crystallization and phase identification were possible. Two setups were used for

Table 1
Deposition parameters used for preparing each sample.

Sample	TmO#1	TmO#2	TmON#1	TmON#2	TmON#3	TmN#1
N_2 Flow (sccm)	–	–	10.0	10.0	10.0	10.0
O_2 Flow (sccm)	1.2	1.8	–	0.2	1.0	–
Ar Flow (sccm)	30.8	30.2	22.0	21.8	21.0	22.0
Power (W)	40	40	20	20	20	30
Dep. Time (h)	12	12	9	12	9	9

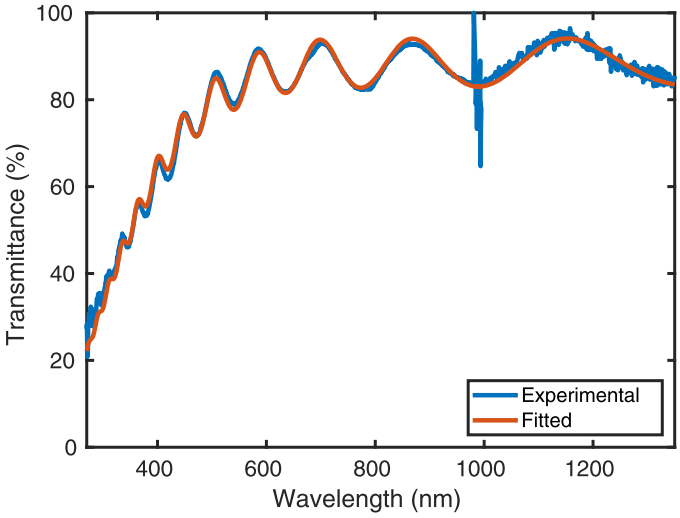

Figure 2. Transmission spectrum of Tm_2O_3 (sample TmO#1) is in blue. In red is a simulated transmission using the retrieved values of n (λ=585 nm) = 1.81, d = 969nm. The transmission spectrum consists of two spectra measured by different CCD spectrometers covering, separately the VIS and the NIR regions. The separate spectra are merged during post-processing. More details on the data acquisition is in section 2.

thermal processing. A Surface Science Integration Solaris 100 Rapid Thermal Processing (RTP) unit was used to anneal the oxide films (TmO#1 and TmO#2) in Argon at 1200°C. Tm (oxy)nitride films (TmON#1, TmON#2, TmON#3, and TmN#1), which oxidize when exposed to air, were annealed in Ar at 4.3 Pa within the AJA ATC Orion 5 sputter system in three rounds of 15 min at 800°C right after deposition. This system uses two halogen lamps on the back of the substrate holder as heat source. Except from TmON#1, the remaining (oxy)nitride films were transferred in a vacuum sealed transfer unit to a glovebox.

3. Results and Discussion

Figure 3 shows three reactive sputtering hysteresis curves of the metallic thulium target under oxygen flow. From top to bottom, they represent the target voltage, deposition rate, and Tm optical emission intensity. Despite the complex behaviour shown in plasma emission curve, this observation was reproducible on several repetitions of the process. The discussion of this complex behaviour of the Tm optical emission hysteresis curve is outside the scope of this contribution. The voltage hysteresis curve shows that the first critical point occurs around 1.3 sccm. The first critical point is defined as the reactive gas flow (upon increasing amount of reactive flow) in which the target makes the transition from the metallic to the compound deposition. Despite all noise obtained in the metallic region of the hysteresis curve, the deposition rate curve was above 3 Å/s. For the oxides, the deposition rate decreased to around 0.2 Å/s.

The O_2 flows used for depositing samples TmO#1 and TmO#2 are also highlighted. In agreement with the transmission results, TmO#1, prepared close to the first critical point, thus an intermediary region, resulted in a Tm oxide film with a sub-stoichiometric character. The observed optical bandgap of TmO#1 is 3.0 eV - significantly below what is observed in the sesquioxide film, TmO#2, which has an optical bandgap of 4.5 eV. According to Rogers et al. [24], Tm_2O_3 has a bandgap of about 5.2 eV. The optical bandgap shows significant change depending on the film composition. Notice, however, that the optical bandgap definition used by Rogers et al. is different from the one adopted here. In Rogers et al. work, the bandgap energy value adopted was the more subjective wavelength energy of onset to high diffuse reflectance of the materials. It is well known that the Tauc bandgap definition can underestimate the optical bandgap [25]. Table 2

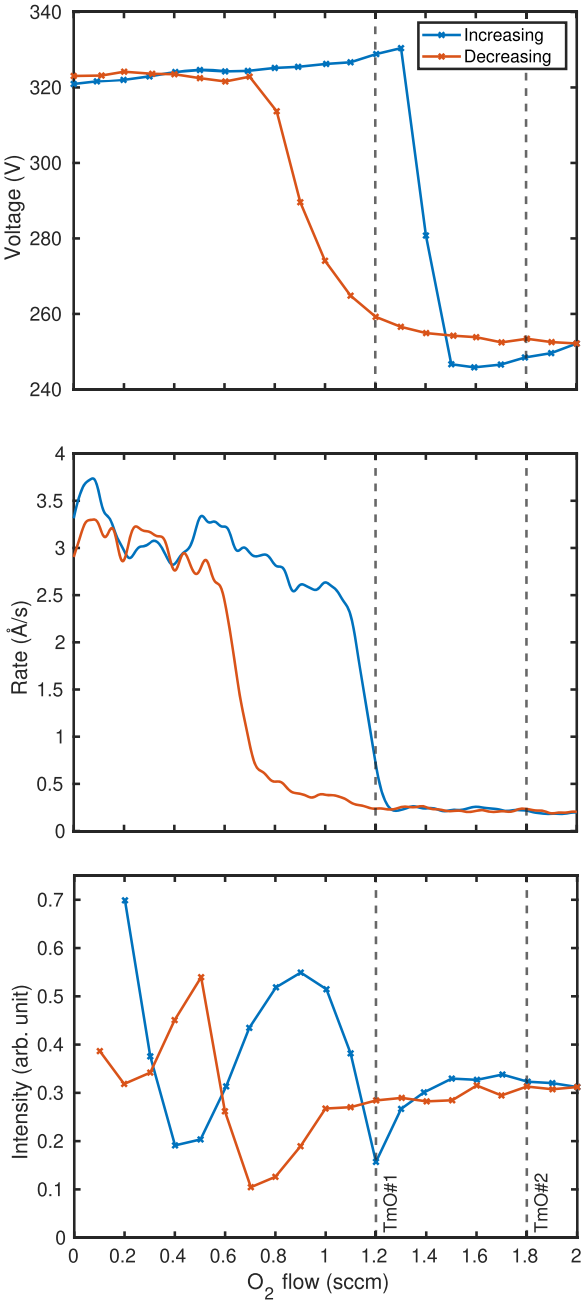

Figure 3. Hysteresis curves of Tm metal target under the flow of O_2. From top to bottom, these graphs represent respectively target voltage, deposition rate, and plasma emission intensity. In blue is the curve generated by increasing the reactive gas flow from the metallic mode. In red the curve generated by reducing the reactive gas flow starting at the compound mode. The black circle marks the conditions used for the deposition of film TmO#1 and the red X marks the condition used for the deposition of film TmO#2. Further details are in section 2.

summarizes the observed composition and optical characteristics of each. EDS results confirm this and reveal that sample TmO#1 is a sub-oxide film, with an oxygen to thulium ratio of about 1.1, significantly lower than a fully oxidized Tm_2O_3 (TmO#2). XRD measurements show that the films are initially amorphous-like (see figure 4 for the XRD results of TmO#2). After RTP annealing, sample TmO#2 assumes the crystal structure of Tm_2O_3 (ICDD 04-006-5406) with presence of microcrystalline structures due to the presence of broad diffraction peaks. The broad peak centred about 21° is related to the glassy quartz substrate and not to the film.

Table 2
Summary of the optical properties and composition of the films. The optical properties (refractive index, optical bandgap, and thickness) were determined from transmission experiments. Oxygen and nitrogen atomic ratios to thulium were determined from EDS.

Sample	TmO#1	TmO#2	TmON#1	TmON#2	TmON#3	TmN#1
n @ 585 nm	1.81	1.67	2.24	1.85	1.64	2.46
E_{Tauc} (eV)	3.0	4.5	2.0	4.4	3.8	1.5
d (nm)	969	369	696	347	269	690
Dep. Rate (nm/s)	0.022	0.008	0.020	0.008	0.040	0.500
[O]/[Tm]	1.1	1.5	1.0	1.1	–	–
[N]/[Tm]	–	–	0.3	0.1	–	–

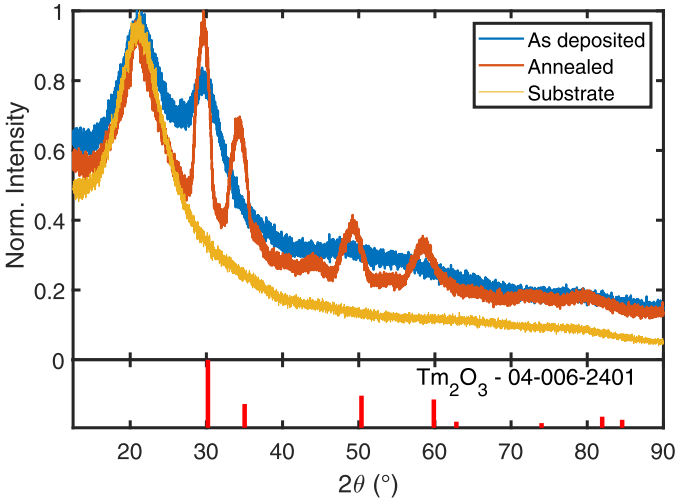

Figure 4. Normalized θ-2θ x-ray diffraction scan of sample TmO#2 before (in blue) and after annealing at 1000°C (in red). Reference lines of the phase given by ICDD 04-006-240 of Tm_2O_3 are shown in red below. The broad peak centred about 21° is related to the glassy UV grade quartz substrate used (in yellow).

Figure 5 shows the hysteresis curves of the reaction of the Tm metallic target with nitrogen. From top to bottom, the graphs show, respectively, the target voltage, deposition rate, and Tm optical emission intensity. Differently from the reactive sputtering with oxygen, nitrogen does not show a strong hysteresis effect. The curve obtained from optical emission of Tm shows different hysteresis effects compared to the hysteresis curves built by monitoring the voltage at the target and deposition rate. In order to document the oxidation of TmN film under air conditions, two films (TmN#1 and TmON#1) were prepared on the compound region of the poisoning regime. Both films were annealed at 800°C inside the sputter coater but film TmON#1 was deliberately exposed to air and subsequently characterized by EDS. Film TmN#1 was sealed in a vacuum sealed sample holder. From EDS characterization (see figure 6), film TmON#1 retained part of its nitrogen but reacted severely with O, assuming an average [N]/[Tm] and [O]/[Tm] ratios of, respectively, about 0.3 and 1.0. Film TmN#1 was characterized by XRD measurements after crystallization due to annealing treatment at the sputter chamber at 800°C as described in section 2. Figure 7 shows its XRD pattern and show a diffraction signature consistent with TmN ICDD 04-006-6487.

Rogers et al. [24] predicted an optical bandgap of 1.8 eV for TmN. The measured optical bandgap as calculated with a Tauc plot was found to be 1.5 eV (see film TmN#1 in figure 8). Even with the systematic underestimation, characteristic of the Tauc method in determining the optical bandgap value compared with the method in [24], the hysteresis behaviour of the Tm target under reaction with N does not reach a plateau with high N_2 flow, which appears to be a characteristic situation where the target is fully poisoned [14]. Thus, it seems plausible to assume that TmN#1 cannot be completely nitrified, so the possibility of film TmN#1 being a mixture of an amorphous network with

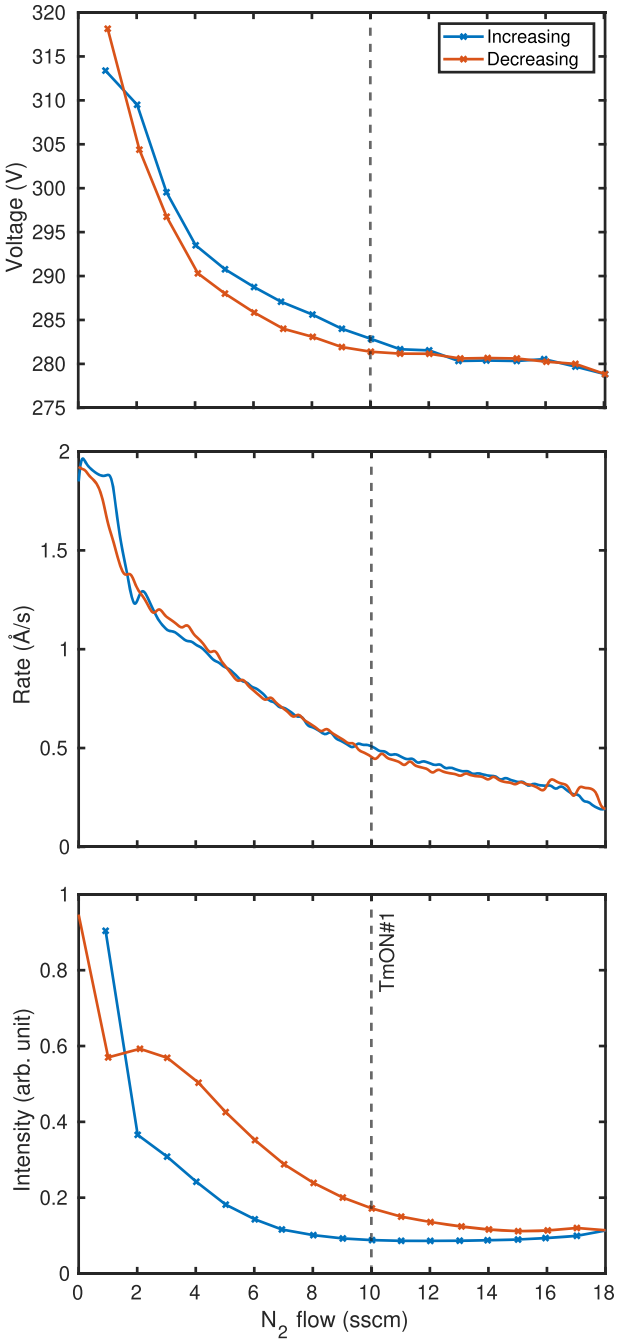

Figure 5. Hysteresis curves of Tm metal target under the flow of N_2. From top to bottom, these graphs represent respectively target voltage, deposition rate, and plasma emission intensity. The curve in blue was generated by increasing the reactive gas flow from the metallic mode. In red is the curve generated by reducing the reactive gas flow starting at the compound mode. The dashed line marks the conditions used for the deposition of films TmON#1 and TmN#1.

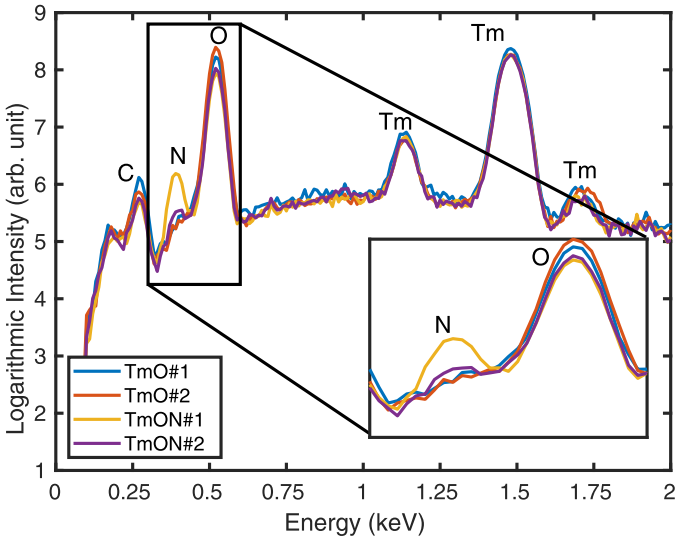

Figure 6. EDS spectra of films TmO#1, TmO#2, TmON#1, and TmON#2, in logarithmic scale. The corresponding X-ray characteristic lines of each constituent element is also shown. Films TmON#3 and TmN#1 were not characterized by EDS and are not shown. All spectra show the presence of adventitious carbon.

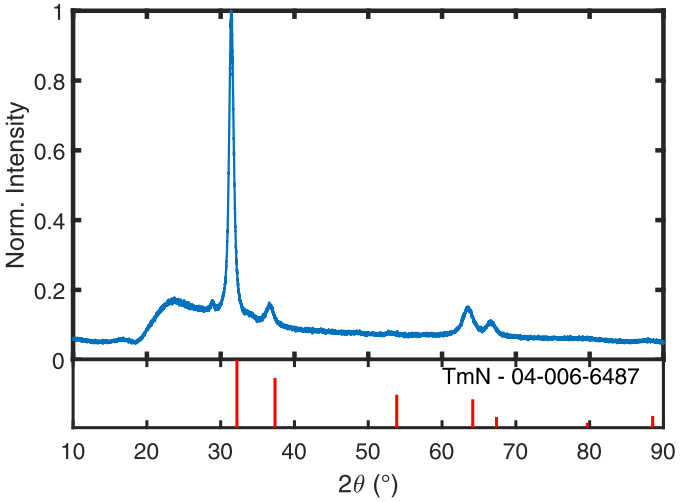

Figure 7. Normalized θ-2θ X-ray diffraction scan of sample TmN#1 (upper graph). In red is the normalized TmN reference lines of ICDD card 04-006-6487.

sub-stoichiometric character and crystalline TmN cannot be completely ruled out. Film TmON#1, by contrast, showed a slightly wider optical bandgap (2.0 eV) due to its oxidation in air as shown by EDS results (see film TmON#1 in figure 6).

Other two oxynitride thin films were prepared with a mixture of N_2 and O_2 (samples TmON#2 and TmON#3) with a very low O_2 flow. Sample TmON#2 was exposed to air and therefore characterized by EDS while sample TmON#3 remained under vacuum conditions. While for the air exposed TmN film (sample TmON#1) the nitrogen amount is significantly higher, sample TmON#2 showed only trace amounts of N. This is corroborated by optical absorption ($E_{Tauc} = 4.4$ eV) and refractive index ($n = 1.85$) values, resembling those found in sesquioxide ($n = 1.67$ and $E_{Tauc} = 4.5$ eV for sample TmO#2). Sample TmON#3 has an E_{Tauc} of about 3.8 eV indicating that it has an even higher amount of N, possibly higher than the one observed in sample TmON#2 due to its prevention of air exposure. Because an EDS characterization in sample TmON#3 would require air exposure, a more precise determination of [N]/[Tm] ratio is not reported.

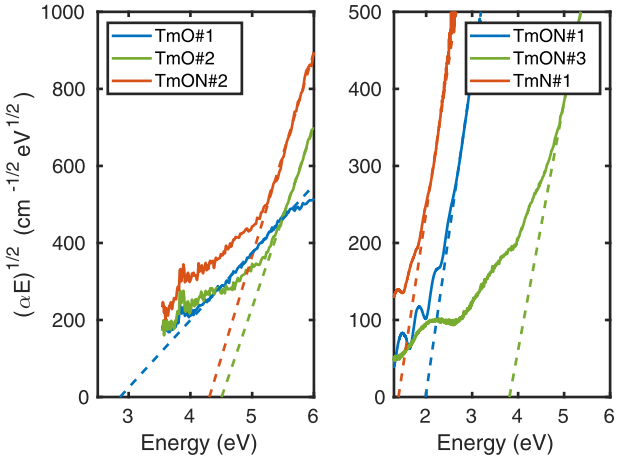

Figure 8. Tauc plots of all films and their respective linear fits. The intersect of the linear fits to the energy axis represent the Tauc bandgaps. In the left is a Tauc plot in the VUV region. They are representative of the oxide films. The right graph shows Tauc plots in the UV-VIS region, representative of the nitride and oxynitride films.

4. Summary and Conclusion

This work reports on structural and optical properties of Tm_2O_3, TmN, and TmO_xN_y thin films prepared by DC reactive magnetron sputtering.

In total, two oxide films, one TmN film, and three films with intermediate oxynitride compositions were fabricated. We also report refractive index, optical bandgap, and composition information as characterized by transmission, EDS for the oxides, and XRD measurements for the nitrides.

Hysteresis curves, a characteristic of the reaction of the sputter gas composition with the metallic Tm target, were also characterized. They were obtained simultaneously from measurements of the voltage at the target, deposition rate, and from Tm plasma emission intensity. Thulium oxide and nitride with different stoichiometry were associated to different regions on the hysteresis curve. Thin films with a thulium oxynitride character could be prepared either by reaction of a pure TmN film with air, or by introducing small oxygen amounts for reaction at the sputter chamber. All films have an amorphous character in as deposited condition and start crystallizing after annealing at temperatures starting at 800°C. Thulium oxide crystallizes in the ICDD 04-006-5406 phase and the reported thulium nitride film crystallizes in the ICDD 04-006-6487 phase.

CRediT authorship contribution statement

Axel Meeuwissen: Investigation, Data curation, Software, Writing - original draft. **Giacomo B.F. Bosco:** Conceptualization, Supervision, Project administration, Writing - review & editing. **Erik van der Kolk:** Funding acquisition, Resources, Supervision, Writing - review & editing.

Declaration of Competing Interest

The authors declare having no competing financial or competing interest which could have influenced the work reported.

Acknowledgement

This work is part of the research LIFT-HTSM 2017 program and was financially supported by 'Nederlandse Organisatie voor Wetenschappelijk Onderzoek (NWO)' – Grant No. 680-91-201.

References

[1] M. Kouda, T. Kawanago, P. Ahmet, K. Natori, T. Hattori, H. Iwai, K. Kakushima, A. Nishiyama, N. Sugii, K. Tsutsui, Interface and electrical properties of Tm_2O_3 gate dielectrics for gate oxide scaling in MOS devices, J. Vac. Sci. Technol. B, Nanotechnol. Microelectron. Mater. Process. Meas. Phenom. 29 (2011), 062202. https://doi.org/10.1116/1.3660800.

[2] J. Singh, A. Roychoudhury, M. Srivastava, P.R. Solanki, D.W. Lee, S.H. Lee, B. D. Malhotra, A dual enzyme functionalized nanostructured thulium oxide-based interface for biomedical application, Nanoscale 6 (2014) 1195–1208. https://doi.org/10.1039/C3NR05043B.

[3] J.J. Wang, Z.B. Fang, T. Ji, W.Y. Ren, Y.Y. Zhu, G. He, Band offsets of epitaxial Tm2O3 high-k dielectric films on Si substrates by X-ray photoelectron spectroscopy, Appl. Surf. Sci. 258 (2012) 6107–6110. https://doi.org/10.1016/j.apsusc.2012.03.013.

[4] I.Z. Mitrovic, M. Althobaiti, A.D. Weerakkody, N. Sedghi, S. Hall, V.R. Dhanak, P. R. Chalker, C. Henkel, E. Dentoni Litta, P.-E. Hellström, M. Östling, Interface engineering of Ge using thulium oxide: Band line-up study, Microelectron. Eng. 109 (2013) 204–207. https://doi.org/10.1016/j.mee.2013.03.160.

[5] I.Z. Mitrovic, S. Hall, M. Althobaiti, D. Hesp, V.R. Dhanak, A. Santoni, A. D. Weerakkody, N. Sedghi, P.R. Chalker, C. Henkel, E. Dentoni Litta, P.-E. Hellström, M. Östling, H. Tan, S. Schamm-Chardon, Atomic-layer deposited thulium oxide as a passivation layer on germanium, J. Appl. Phys. 117 (2015), 214104. https://doi.org/10.1063/1.4922121.

[6] H. Yoshitomi, S. Kitayama, T. Kita, O. Wada, M. Fujisawa, H. Ohta, T. Sakurai, Optical and magnetic properties in epitaxial GdN thin films, Phys. Rev. B - Condens. Matter Mater. Phys. 83 (2011) 1–7. https://doi.org/10.1103/PhysRevB.83.155202.

[7] D.P. Schumacher, W.E. Wallace, A.W.E. Wallace, Magnetic Characteristics of Gadolinium, Praseodymium, and Thulium Nitrides, Mech. Electrolytic Oxid. Alum. J. Appl. Phys. 36 (1965) 477. https://doi.org/10.1063/1.1714289.

[8] N. Sclar, Properties of Rare-Earth Nitrides, J. Appl. Phys. 35 (1964) 1534–1538. https://doi.org/10.1063/1.1713662.

[9] J.W. Gerlach, J. Mennig, B. Rauschenbach, Epitaxial gadolinium nitride thin films, Appl. Phys. Lett. 90 (2007) 61919. https://doi.org/10.1063/1.2472538.

[10] J.H. Richter, B.J. Ruck, M. Simpson, F. Natali, N.O.V Plank, M. Azeem, H. J. Trodahl, A.R.H. Preston, B. Chen, J. Mcnulty, K.E. Smith, A. Tadich, B. Cowie, A. Svane, M. Van Schilfgaarde, W.R.L. Lambrecht, Electronic structure of EuN: Growth, spectroscopy, and theory, Phys. Rev. B. 84 (2011), 235120. https://doi.org/10.1103/PhysRevB.84.235120.

[11] E.-M. Anton, B.J. Ruck, C. Meyer, F. Natali, H. Warring, F. Wilhelm, A. Rogalev, V. N. Antonov, H.J. Trodahl, Spin/orbit moment imbalance in the near-zero moment ferromagnetic semiconductor SmN, Phys. Rev. B. 87 (2013), 134414. https://doi.org/10.1103/PhysRevB.87.134414.

[12] B.J. Ruck, H.J. Trodahl, J.H. Richter, J.C. Cezar, F. Wilhelm, A. Rogalev, V. N. Antonov, B. Do Le, C. Meyer, Magnetic state of EuN: X-ray magnetic circular dichroism at the Eu $M_{4,5}$ and $L_{2,3}$ absorption edges, Phys. Rev. B. 83 (2011), 174404. https://doi.org/10.1103/PhysRevB.83.174404.

[13] F. Natali, B.J. Ruck, N.O.V. Plank, H.J. Trodahl, S. Granville, C. Meyer, W.R. L. Lambrecht, Rare-earth mononitrides, Prog. Mater. Sci. 58 (2013) 1316–1360. https://doi.org/10.1016/j.pmatsci.2013.06.002.

[14] K. Strijckmans, R. Schelfhout, D. Depla, Tutorial: Hysteresis during the reactive magnetron sputtering process, J. Appl. Phys. 124 (2018), 241101. https://doi.org/10.1063/1.5042084.

[15] S. Berg, T. Nyberg, Fundamental understanding and modelling of reactive sputtering processes, Thin Solid Films 476 (2005) 215–230. https://doi.org/10.1016/j.tsf.2004.10.051.

[16] N.A.T. A. Kramida, Yu. Ralchenko, J. Reader, NIST Standard Reference Database, V5.7.1, (2019). https://doi.org/10.18434/T4W30F.

[17] B.L. Henke, E.M. Gullikson, J.C. Davis, X-ray interactions: photoabsorption, scattering, transmission, and reflection at E=50-30000 eV, Z=1-92, Atomic Data and Nuclear Data Tables 54 (no.2) (July 1993) 181–342. https://doi.org/10.1006/adnd.1993.1013.

[18] E.P.J. Merkx, E. van der Kolk, Method for the Detailed Characterization of Co-sputtered Inorganic Luminescent Material Libraries, ACS Comb. Sci. 20 (2018) 595–601. https://doi.org/10.1021/acscombsci.8b00068.

[19] R. Alvarez, A. Garcia-Valenzuela, C. Lopez-Santos, F.J. Ferrer, V. Rico, E. Guillen, M. Alcon-Camas, R. Escobar-Galindo, A.R. Gonzalez-Elipe, A. Palmero, High-Rate Deposition of Stoichiometric Compounds by Reactive Magnetron Sputtering at Oblique Angles, Plasma Process. Polym. 13 (2016) 960–964. https://doi.org/10.1002/ppap.201600019.

[20] R. Swanepoel, Determination of the thickness and optical constants of amorphous silicon, J. Phys. E. 16 (1983) 1214–1222. https://doi.org/10.1088/0022-3735/16/12/023.

[21] B. Tatian, Fitting refractive-index data with the Sellmeier dispersion formula, Appl. Opt. 23 (1984) 4477. https://doi.org/10.1364/AO.23.004477.

[22] D. Poelman, P.F. Smet, Methods for the determination of the optical constants of thin films from single transmission measurements: a critical review, J. Phys. D. Appl. Phys. 36 (2003) 1850–1857. https://doi.org/10.1088/0022-3727/36/15/316.

[23] I.H. Malitson, Interspecimen Comparison of the Refractive Index of Fused Silica, J. Opt. Soc. Am. 55 (1965) 1205. https://doi.org/10.1364/JOSA.55.001205.

[24] E. Rogers, P. Dorenbos, E. van der Kolk, Systematics in the optical and electronic properties of the binary lanthanide halide, chalcogenide and pnictide compounds: an overview, New J. Phys. 13 (2011), 093038. https://doi.org/10.1088/1367-2630/13/9/093038.

[25] S.K. Suram, P.F. Newhouse, J.M. Gregoire, High Throughput Light Absorber Discovery, Part 1: An Algorithm for Automated Tauc Analysis, ACS Comb. Sci. (2016) 18. https://doi.org/10.1021/acscombsci.6b00053.